Petrologic imaging of the architecture of magma reservoirs feeding calderaforming eruptions

3

- 5 Benjamin A. Black<sup>1,2</sup> and Benjamin J. Andrews<sup>3</sup>
- <sup>1</sup>Earth and Atmospheric Science, City College of New York, New York, NY 10031. <sup>2</sup>Earth and
- 7 Environmental Sciences, Graduate Center, City University of New York, New York, NY 10017.
- 8 <sup>3</sup>Global Volcanism Program, Smithsonian Institution, Washington, D.C.
- 9 Corresponding author: Benjamin Black (bblack@ccny.cuny.edu)

10

### Abstract

Caldera footprints and erupted magma volumes provide a unique constraint on vertical dimensions of upper crustal magma reservoirs that feed explosive silicic eruptions. Here we define a Vertical Separation (VS) ratio in which we compare the geometric vertical extent with the range of depths indicated petrologically by melt inclusion water and CO<sub>2</sub> saturation pressures for fifteen caldera-forming eruptions spanning ~10<sup>0</sup> km<sup>3</sup> to ~10<sup>3</sup> km<sup>3</sup> in volume. We supplement melt inclusion saturation pressures with rhyolite-MELTS barometry and plagioclase-melt hygrometry to generate a petrologic image of magma reservoir architecture. We find that preeruptive upper crustal magma reservoirs range from contiguous bodies (where petrologic and geometric estimates match closely) to vertically dispersed structures. Vertically dispersed preeruptive reservoirs are more common among intermediate-volume eruptions than among the smallest and largest caldera-forming eruptions. We infer that the architecture of magma reservoirs tracks the thermomechanical evolution of large volcanic systems.

### 1. Introduction

The largest silicic eruptions evacuate magma reservoir systems that can exceed 10<sup>3</sup> km<sup>3</sup> in volume. Such eruptions, accompanied by caldera collapse (Lipman, 1997), fundamentally restructure magma plumbing systems (Barker et al., 2015; Andrews and Gardner, 2010), contributing to a dearth of exposed storage systems that can be directly linked to eruptions. Models for large magma bodies differ on the timescales of assembly and the thermal and rheological state of the magma during assembly and storage (e.g., Michaut and Jaupart, 2006; Eddy et al., 2016; Huber et al., 2019). Key unresolved questions include the vertical structure of upper crustal magma reservoirs (e.g., Cashman et al., 2017), how plumbing systems influence eruptions, and whether the organization of individual magma bodies is static or evolves during the lifetime of the overall magmatic system (e.g., Gualda et al., 2018).

These questions matter because reservoir structure relates directly to understanding the largest explosive eruptions on Earth and the relationship between volcanic and plutonic rocks (Bachmann and Bergantz, 2008; Cashman and Giordano, 2014). Rapid reorganization of magmatic systems and assembly of eruptible melt-rich bodies has been linked to triggering of large eruptions (Druitt et al., 2012; Allan et al., 2013). Proposed models for silicic magma systems range from large, compositionally zoned, integrated magma bodies undergoing unified thermal evolution, crystallization, and differentiation (Hildreth, 1981), to multiple, spatially juxtaposed but compositionally distinct magma bodies (Cooper et al., 2012), to spatially and compositionally discrete magma lenses that integrate prior to or during eruption (Cashman et al., 2017). In all of these conceptual models, the upper crustal plumbing system is only the

shallowest portion of a magmatic system that extends into deep hot zones near the base of the crust (e.g., Annen et al., 2006).

Caldera-forming eruptions offer a unique opportunity to investigate the vertical structure and evolution of upper crustal magmatic plumbing systems, because the caldera footprint itself preserves a record of the lateral scale of the evacuated portion of a magma reservoir (Cashman and Giordano, 2014). We use this horizontal scale, together with estimates of erupted volume, to calculate the vertical dimension of a hypothetical magma chamber consisting of a 'big tank' containing only the magma that erupted. We compare this implied vertical dimension with the vertical drainage height revealed by the observed range in melt inclusion saturation pressures. This petrologic imaging exposes rich, scale-dependent diversity in the vertical organization of natural upper crustal magma reservoirs. In particular, the largest and smallest magma bodies tend towards consolidated structures. We explore hypotheses to explain consolidation of large-scale magma chambers, including selective eruption of shallow large magma bodies with low roof aspect ratios, upward migration of dispersed magma lenses, or emplacement of successive magma bodies progressively occupying the upper crust. We discuss the relationship between thermomechanical regime and reservoir structure to understand pathways for evolution of magmatic architecture through the life cycle of the magmatic system.

# 2. Materials and Methods

49

50

51

52

53

54

55

56

57

58

59

60

61

62

63

64

65

66

67

68

69

70

# 2.1 The Vertical Separation ratio

We compiled caldera collapse areas ( $A_{collapse}$ ), erupted volumes ( $V_{erupted}$ ), and melt inclusion  $H_2O-CO_2$  data from fifteen silicic caldera-forming eruptions ranging in dense-rock equivalent (DRE) erupted volume from  $10^0-10^3$  km<sup>3</sup> (see Table S1 for complete database and

data sources). Following Cashman and Giordano (2014), we used these datasets to calculate the vertical extent, h, implied by a consolidated tank-like geometry:

$$h=V_{erupted}/A_{collapse}$$
 (1)

where  $V_{erupted}$  is the DRE volume including fall, ignimbrite, and intracaldera deposits. This vertical extent is a simplification as it represents the vertical dimension of a cylinder of magma with a horizontal area equal to that of the caldera and a volume equal to that of the erupted deposits. We suggest that melt inclusion saturation pressures reflect a more realistic view of the true vertical extent of the magma reservoirs that participated in an eruption (Cashman and Giordano, 2014). We call the ratio between the vertical extent from petrologic records of pressure ( $h_{pet}$ , from melt inclusions or rhyolite-MELTS for example) relative to the consolidated vertical extent (h) the Vertical Separation (VS) ratio:

82 
$$VS = h_{pet}/h$$
. (2)

This ratio captures the dispersion of a given reservoir system relative to a compact, contiguous magma body (Figure 1).

Caldera collapse areas and eruption volumes are known primarily from geologic mapping (e.g., Geyer and Marti, 2008; Cashman and Giordano, 2014). Eq. 1 assumes that the collapse area reflects the horizontal extent of the reservoir from which magma was extracted. Although some small calderas do root in funnel-like geometries (Lipman, 1997), this assumption is consistent with multidisciplinary investigation of caldera formation (Gudmundsson et al., 2016). On the other hand, lateral movements of magmas during eruptions, such as those thought to have taken place during the 1912 Katmai eruption (e.g., Hildreth and Fierstein, 2000) and possibly the Bishop Tuff eruption (Cashman and Giordano, 2014), show that there are some exceptions to this assumption (see also Kennedy et al., 2018). Significant lateral extraction from

outside the collapse footprint would imply that  $A_{collapse}$  and thus VS are underestimates. In this work, we address the portions of the reservoir that participate in eruption. For smaller eruptions, this may represent a fraction of the overall reservoir volume, but for eruptions larger than  $\sim \! 10$  km<sup>3</sup>, the caldera radius is likely to be a good approximation of the reservoir radius (Karlstrom et al., 2012).

# 2.2 Pre-eruptive storage pressures

Pre-eruptive storage pressures can be estimated from experimental petrology (e.g., Andrews and Gardner, 2010), from thermodynamic calculations of phase equilibria (e.g., Gualda and Ghiorso, 2014; Gualda et al., 2018), or from water and CO<sub>2</sub> concentrations in melt inclusions (e.g., Newman and Lowenstern, 2002), taking advantage of the pressure-dependence of water and CO<sub>2</sub> solubility in silicate glasses. Here we focus on melt inclusion saturation pressures because water and CO<sub>2</sub> data from multiple inclusions in multiple samples are available for a large number of caldera-forming eruptions, permitting insights into the range of estimated storage pressures and facilitating direct comparison among magmatic systems. We use pressures calculated with rhyolite-MELTS based on phase equilibria (Gualda and Ghiorso, 2014; Bégué et al., 2014; Gualda et al., 2018) as an independent point of comparison with the melt inclusion data.

Melt inclusion data (Supplementary Table 1) are from Bacon and Druitt (1988), Lowenstern (1993), Wallace and Gerlach (1994), Wallace et al. (1999), Marianelli et al. (2006), Di Muro et al. (2006), Mandeville et al. (2009), Smith et al. (2010), Chesner and Luhr (2010), Bachmann et al. (2010), Johnson et al. (2011), Cadoux et al. (2014), Bégué et al. (2015),

Iacovino et al. (2016), and Myers et al. (2016). Uncertainties in  $H_2O$  and  $CO_2$  measurements via FTIR and SIMS are similar, with 2-sigma uncertainties typically in the range of ~10-20% for  $H_2O$  and 5-10% for  $CO_2$ . These uncertainties in in  $H_2O$  and  $CO_2$  concentrations translate to 2-sigma uncertainties of ~15-25% in pressure estimates. In cases where saturation pressure estimates do not accompany water and  $CO_2$  data, we compute saturation pressures using the VolatileCalc software (Newman and Lowenstern, 2002).

117

118

119

120

121

122

123

124

125

126

127

128

129

130

131

132

133

134

135

136

137

138

139

Calculation of saturation pressures from melt inclusions necessitates a number of assumptions. We assume that water and CO<sub>2</sub> concentrations reflect pre-eruptive magma storage and equilibration pressures rather than entrapment pressures, because water diffusion through host crystals allows melt inclusions to re-equilibrate on timescales of several years at magmatic temperatures (e.g., Qin et al., 1992). Conversion of water and CO<sub>2</sub> concentrations to pressures assumes volatile saturation (Newman and Lowenstern, 2002), implying that our estimates give a lower limit on the vertical extent of the system. However, abundant evidence points to volatile saturation prior to eruption. Examples include excess sulfur in eruptions like that of Mount Pinatubo (e.g., Wallace and Gerlach, 1994; Iacovino et al., 2016) and trace element trends in the Bishop Tuff (Wallace et al., 1999). Melt inclusions can also record degassing during ascent rather than storage conditions. For example, some of the spread in H<sub>2</sub>O concentrations in Huckleberry Ridge Tuff melt inclusions has been attributed to variable degassing and diffusive loss during magma ascent (Myers et al., 2016). We therefore rely on reconstructed H<sub>2</sub>O concentrations and storage pressures from Myers et al. (2016). In general, the sensitivity of our results to melt inclusion degassing is limited in that most of the systems considered here are thought to be stored at shallow (i.e., upper crustal) depths based on a range of independent barometers and experimental data. An additional possibility is that some melt inclusions in

crystal rims may be anomalous due to boundary layer effects during rapid crystallization (Pamukcu et al., 2016). Consequently, to reduce the sensitivity of our calculations to any outliers, we calculate VS ratios after discarding outliers defined as data points more than 1.5 interquartile ranges below or above the 1<sup>st</sup> and 3<sup>rd</sup> quartile, respectively (Figure 2; Supplementary Table 1).

140

141

142

143

144

145

146

147

148

149

150

151

152

153

154

155

156

157

158

159

160

161

162

Accurate pressure estimates from water-CO<sub>2</sub> saturation depend on accurate determination of dissolved pre-eruptive CO<sub>2</sub> concentrations. Vapor bubbles that form after melt inclusion entrapment often contain a majority of the initially dissolved CO<sub>2</sub> (e.g., Moore et al., 2015; Aster et al., 2016). Among the melt inclusion sample suites included here, eight of fifteen focused on melt inclusions in which bubbles were rare to absent (Table 1). Marianelli et al. (2014) and Iacovino et al. (2016) performed homogenization experiments to re-dissolve vapor bubbles in the melt. Iacovino et al. (2016) found that re-incorporation of vapor bubbles accounted for ≤ 23 ppm CO<sub>2</sub>, consistent with shallow storage conditions of Paektu magma as inferred from stable phase assemblages and depths of seismicity. Among the five melt inclusion suites in which bubbles were either not described or were common features, three (Katmai, Santorini, Laacher See) originated from relatively shallow reservoirs as independently substantiated with experimental data (e.g., Cadoux et al., 2014) and consisted of melt inclusions with CO<sub>2</sub> below detection limits (<10-50 ppm) in the glass, implying that post-entrapment growth of CO<sub>2</sub>-rich vapor bubbles is unlikely. For eruptions such as Rotoiti, where melt inclusions can contain tiny vapor bubbles (Bégué et al., 2015), if these bubbles contain a significant quantity of originally dissolved CO<sub>2</sub> the consequence would be a larger range in storage pressures and thus a higher VS ratio. In such cases the VS ratios we calculate may represent conservative values. CO<sub>2</sub>-rich flushing can alter dissolved water and CO<sub>2</sub> concentrations (e.g., Caricchi et al., 2018). However, the combined water-CO<sub>2</sub> equilibria still reflect the pressure dependence of water and CO<sub>2</sub> solubility, barring the presence of substantial unaccounted-for CO<sub>2</sub> in vapor bubbles.

165

166

167

163

164

2.3 Comparison with water concentrations from plagioclase-melt equilibria and with storage pressures from rhyolite-MELTS phase equilibria

168

169

170

171

172

173

174

175

176

177

178

179

180

181

182

183

184

185

To investigate the evolution of reservoirs prior to pre-eruptive melt inclusion reequilibration, we compiled measurements of plagioclase compositions for five of the calderaforming eruptions in our dataset (Pinatubo, Santorini, Rotoiti, Oruanui, Bishop) (Hattori and Sato, 1996; Wilson et al., 2005; Smith et al., 2010; Druitt et al., 2012; Cadoux et al., 2014; Chamberlain et al., 2015). We concentrated on eruptions for which plagioclase measurement locations were constrained to crystal cores and rims. We used the plagioclase rim compositions in conjunction with matrix glass compositions to calculate equilibrium magmatic water concentrations with the updated plagioclase-liquid hygrometer of Waters and Lange (2015), which describes how higher anorthite contents in plagioclase record higher magmatic water contents at a given temperature. Temperature inputs for each unit are summarized in Table 2. For all but one eruption (that of the Campanian Ignimbrite), the available temperature estimates derive primarily from Fe-Ti oxides. We note that Fe-Ti oxides re-equilibrate very rapidly—in days to weeks—at magmatic temperatures (Venezky and Rutherford, 1999), thus they are not sensitive to longer-term variation in magmatic storage temperature. To account for some of the uncertainty in temperature estimates, we consider both the upper and lower end of available temperature estimates. We found sensitivity to pressure to be negligible, and therefore selected the lower end of available storage estimates to obtain conservative estimates of magmatic water concentrations. Selecting the highest estimated storage pressures for each eruption does not alter the results (Supplementary Table 2). We compare the water concentrations inferred from plagioclase compositions with water concentrations in melt inclusions from the same units. In contrast to rapid re-equilibration of melt inclusion water contents at magmatic temperatures (e.g., Qin et al., 1992), CaAl-NaSi interdiffusion in plagioclase takes place very slowly due to the coupled substitution required to maintain charge balance (e.g., Grove et al., 1984). Plagioclase rims thus have the capacity to retain a longer-term history of magmatic water than melt inclusions because plagioclase compositions are unlikely to re-equilibrate in response to degassing.

We do not estimate pressures based solely on water concentrations from the plagioclase-melt hygrometer owing to potential uncertainties due to the lack of a constraint on CO<sub>2</sub>. Instead, we use pressures calculated with rhyolite-MELTS phase equilibria (Ghiorso and Gualda, 2014; Bégué et al., 2014; Gualda et al., 2018) as independent points of comparison with melt inclusion saturation pressures. Gualda and Ghiorso (2014) used the pressure-dependence of the quartz and feldspar saturation surfaces to develop a new crystallization pressure barometer for rocks that preserve glass compositions that reflect equilibrium between melt, quartz, and one or two feldspars. The pressure that yields the requisite intersection of these saturation surfaces can be calculated with rhyolite-MELTS (Gualda et al., 2012). Pressures estimated via this approach are independent of melt inclusion H<sub>2</sub>O and CO<sub>2</sub>. Pressure estimates from each method are in good agreement overall, though in some cases pressure estimates from rhyolite-MELTS can differ slightly from melt inclusion H<sub>2</sub>O and CO<sub>2</sub> saturation pressures, possibly due to changes in melt composition during decompression (Gualda and Ghiorso, 2014). We use the pressures tabulated in Ghiorso and Gualda (2014), Bégué et al. (2014), and Gualda et al. (2018) for the Ohakuri,

Mamaku, Rotoiti, Oruanui, Bishop, and Toba eruptions to calculate VS ratios, as detailed in Tables S1 and S3. Where available, we used pressures determined using matrix glass compositions, based on the assumption that matrix glass compositions are more consistent with pre-eruptive storage conditions as reflected in melt inclusion saturation pressures.

### 3. Results

# 3.1 Vertical structure of magma reservoirs

Our analysis of petrologically determined storage pressures illustrates the fundamental diversity of the magma reservoirs that feed caldera-forming eruptions, which range from highly consolidated bodies to vertically dispersed systems. These diverse structures of magma storage are apparent both from the raw distributions of melt inclusion data (Figure 2) and from our comparison of melt inclusion storage pressures with consolidated vertical extent (Figures 3 and 4). For example, the Bishop Tuff and Oruanui eruptions display unimodal, continuous storage pressure distributions, in agreement with VS ratios close to one, whereas Rotoiti melt inclusions display a multimodal storage pressure distribution, in agreement with a VS ratio much greater than one.

Gaps or modes in the distribution of melt inclusion storage pressures are difficult to interpret due to uncertainties in the completeness of the melt inclusion record, even for large sample sets. However, by comparing the vertical range spanned by melt inclusions with the vertical dimension of a consolidated magma body (Figure 3), we can identify eruptions that tap multiple vertically separated magmatic bodies, because they do not erupt a sufficient volume of magma to continuously span the range of depths from which melt inclusions originate.

We find minimum VS values of ~1 among the eruptions for which we have data (Figure 4), supporting our assumptions regarding melt inclusions and the relationship between caldera and reservoir footprint (VS values <<1 would call these assumptions into question). VS values near unity indicate that pre-eruptive magma reservoirs were vertically compact bodies, perhaps in the form of laterally juxtaposed but compositionally distinct magma bodies (e.g., Cooper et al., 2012). Such consolidated reservoirs are present across the range of eruption volumes, but predominate among the smallest and largest caldera-forming eruptions (Figure 4). Among the largest (>500 km³) magma reservoirs, the exception to this trend towards consolidation is the 2500 km³ Huckleberry Ridge Tuff (HRT), which has a VS value of ~8 and shows a bimodal distribution of storage depths (Myers et al., 2016).

We find maximum VS values of ~10-20 among the eruptions for which we have data (Figure 4). Taken at face value, these ratios imply that over the range in depths from which erupted magma was extracted, only 5-10% of the volume was occupied by extracted magma, with country rocks, cumulates, and untapped magma occupying intervening levels of the crust. Such fragmentary, vertically extensive upper crustal magmatic systems are most prevalent among intermediate-to-large volume explosive eruptions (with VEI ~6-7) rather than supereruptions (VEI  $\geq$  8). Vertically dispersed magmas may aggregate shortly before eruptions, perhaps as part of the destabilization that triggers the eruptions (Cashman et al., 2017). If so, the data in our compilation imply this aggregation must take place more rapidly than the several-year equilibration timescale of rhyolitic melt inclusions at magmatic temperatures (Qin et al., 1992).

3.2 Comparison of melt inclusion storage pressures with pressures from rhyolite-MELTS phase equilibria (Gualda and Ghiorso, 2014)

We calculated VS ratios for the Ohakuri, Mamaku, Rotoiti, Oruanui, Bishop, and Toba eruptions from rhyolite-MELTS barometry (Gualda and Ghiorso, 2014; Bégué et al., 2014; Gualda et al., 2018) as an independent check on VS ratios calculated from melt inclusion H<sub>2</sub>O-CO<sub>2</sub> saturation. Overall, the absolute pressure estimates from rhyolite-MELTS and melt inclusion H<sub>2</sub>O-CO<sub>2</sub> saturation pressure are consistent, with some exceptions. These exceptions include the Ohakuri eruption, for which rhyolite-MELTS estimates extend to lower pressures, and the Oruanui and Toba eruptions, for which rhyolite-MELTS estimates extend to higher pressures (Figure 2; Table S1). Despite these incongruities in absolute pressure for some eruptions, the ranges in pressures (and thus the VS ratios) are generally in good agreement between rhyolite-MELTS and melt inclusion saturation pressure data (Figure 4). This agreement supports the robustness of the VS ratios that form the basis for our interpretations.

3.3 Comparison of melt inclusion water concentrations with magmatic water calculated with the plagioclase-liquid hygrometer of Waters and Lange (2015)

We calculated magmatic water concentrations from plagioclase-melt equilibria using the hygrometer of Waters and Lange (2015). While we used plagioclase rim compositions as most likely to be in equilibrium with matrix glass, calculations performed with plagioclase core compositions as a sensitivity test yielded similar results (Figure 5). Uncertainties in temperature estimates, mainly determined from Fe-Ti oxides (Table 2), introduced significant uncertainties in calculated water concentrations. Within these uncertainties, water concentrations from melt inclusions broadly agree with water concentrations predicted independently from plagioclase rim

compositions (Figure 5). This agreement is not without exceptions. In particular, water concentrations implied by plagioclase compositions from Oruanui, Rotoiti, and early and middle Bishop Tuff appear to be 1-2 wt% higher than water concentrations in melt inclusions. In our comparison between the melt inclusion and hygrometer datasets, we focus on water concentration rather than depth. Estimates of depth from volatile saturation require both H<sub>2</sub>O and CO<sub>2</sub> concentrations. CO<sub>2</sub> concentrations are available for melt inclusions from most of the eruptions considered here, but only water concentrations are predicted by the plagioclase-liquid hygrometer. Therefore any estimates of depth based on water concentrations from the plagioclase hygrometer would represent minimum depths compared with those estimated from melt inclusions.

# 4. Discussion

4.1 Diverse upper crustal magma reservoirs

The VS ratio provides a view of the upper crustal architecture of individual reservoir systems that is consistent with both the full melt inclusion datasets (Figure 2) and with other independent petrologic and geochemical constraints from those systems. For example, the VS ratio indicates that the reservoirs feeding the Rotoiti and climactic Mazama eruptions were particularly vertically complex and extensive; the Rotoiti deposits include evidence for multiple discrete magma batches that participated in the eruption (Schmitz and Smith, 2004), and the climactic Mazama deposits are a classic example of an ignimbrite with a compositional gap between early rhyolite and later, crystal-rich andesite-dacite (e.g., Bacon and Druitt, 1988). To date, geophysical imaging of upper crustal magmatic systems beneath calderas lacks the

resolution to resolve fine-scale vertical structure, but supports the existence of upper crustal magma bodies situated beneath collapse regions of some large systems (e.g., Jaxybulatov et al., 2014). We consider the VS ratio a form of petrologic imaging because it uses petrologic constraints to capture a picture of hidden magmatic systems that is complementary to the view from seismic or other geophysical imaging.

The diversity and apparent size-dependence of the upper crustal structure of silicic caldera-forming magma reservoirs raise questions about the physical factors that govern the vertical structure of pre-eruptive magma bodies, and how reservoir organization evolves as magmatic systems develop and alter the rheology of the surrounding rocks (e.g., Gualda et al., 2018; Huber et al., 2019).

# 4.2 Mechanisms for building and erupting very large, consolidated magma reservoirs

The diverse structures of upper crustal magmatic systems, including in many cases evidence for vertically separated reservoirs tapped during eruptions, are consistent with an emerging view of complex, multi-level transcrustal magmatic systems (e.g., Annen et al., 2006; Cashman and Giordano, 2014; Cashman et al., 2017). However, in this context the vertical compactness of three out of four of the upper crustal reservoirs that feed supereruptions is surprising. This trend is based on only four systems for which data are available (HRT, Bishop, Toba, and Oruanui), and therefore must itself be substantiated by additional saturation pressure data. Nevertheless, we consider some initial hypotheses: (1) selective eruption of shallow, large magma bodies (Gregg et al., 2012), (2) ductile reorganization and consolidation of the largest magmatic systems encouraged by thermal priming, and (3) in-situ assembly of the largest magma

reservoirs through incremental addition of magma batches to a finite volume within the upper crust, leading to near-complete occupation of the region of magma storage and development of a contiguous reservoir.

As the largest magma reservoirs heat the surrounding crust, viscosity decreases, promoting creep that relieves stresses due to magma replenishment (Jellinek and DePaolo, 2003). In this regime, bubble-induced overpressure and roof failure have been proposed as trigger mechanisms (Tait et al., 1989; Gregg et al., 2012; Caricchi et al., 2014; Black and Manga, 2017); each mechanism is sensitive to reservoir depth, and roof failure is sensitive to chamber aspect ratio (Gregg et al., 2012), raising the prospect of selective triggering and eruption of shallow, high aspect-ratio reservoirs. As shown in Figure 6, larger volume eruptions converge towards critical roof aspect ratios, supporting selective eruption of shallow large magma bodies rather than deep or vertically dispersed large magma bodies (Gregg et al., 2012).

Two end-member scenarios describe how these large, shallow magma bodies might develop as consolidated reservoirs. In the first, more dynamic scenario, thermal priming and associated decreases in viscosity favor ductile reorganization. Within an extensive mush-rich system, if some magma lenses are more buoyant, and if compaction timescales are sufficiently fast, consolidation in the upper reaches of the mush system is possible (e.g., Bachmann and Bergantz, 2008; Floess et al., 2019). This is similar to the relatively deep magma extraction and relatively shallow magma storage model discussed by Gualda et al. (2019). Likewise, if magma bodies are buoyant relative to host rocks, warm ductile crust favors local diapirism (e.g., Marsh, 1982), which could take place even during intervals when the magmatic system appears to be mostly quiescent and aseismic (Lu et al., 2000). In the second, more static scenario, if magma addition and heat input is focused within a finite volume of upper crust, this volume will become

fully occupied with magma (Annen, 2009; Michaut and Jaupart, 2006). In this view, a region of the upper crust gradually fills in with successive magma bodies. If these magmas are able to erupt when the system is still fragmentary, the resulting high VS ratios reflect dispersed reservoir systems. Magma chamber modeling shows that magma chambers grow when recharge and relaxation timescales are shorter than cooling timescales (e.g., Degruyter and Huber, 2014; Townsend et al., 2019). Huber et al. (2019) suggest the optimum conditions for magma chamber growth exist in the upper crust from ~1.5 to 2.5 kbar, where warm, viscous crust accommodates magma addition but where occasional eruptions are still possible. Addition of magma thermally primes this incubation region, potentially enabling the magma pile to rapidly thaw through latent heat released when formerly glassy material experiences crystal nucleation and growth when reheated to ~700°C (Michaut and Jaupart, 2006). Eruption of a large magma reservoir that has fully occupied a region of the upper crust will yield low VS ratios, as observed for the Toba, Bishop, and Oruanui eruptions.

Comparison of water concentrations calculated from plagioclase composition with water in melt inclusions offers a test of these two consolidation models. If dynamic consolidation takes place and is more rapid than plagioclase re-equilibration but slower than melt inclusion re-equilibration, and if H<sub>2</sub>O concentrations roughly track pressure as predicted by water solubility models (e.g., Newman and Lowenstern, 2002), the prediction is that H<sub>2</sub>O concentrations from the plagioclase-melt hygrometer should be greater than or equal to H<sub>2</sub>O concentrations in melt inclusions. If, on the other hand, static magma bodies reside at specific levels in the upper crust, H<sub>2</sub>O concentrations from the plagioclase-melt hygrometer should match those in melt inclusions.

We interpret the general agreement between water concentrations from plagioclase compositions and melt inclusions (Figure 5) as evidence for dominantly *in situ* growth of the

largest magma chambers. This interpretation is further supported by the raw melt inclusion distributions in Figure 2, which show that the range of storage depths (at 2-10 km) is broadly consistent across eruptions. Within this range there are fewer gaps in melt inclusion data from the largest volume eruptions, suggesting that magma progressively occupies a preferred storage level (Huber et al., 2019), perhaps as melts percolate out of deeper melt generation and extraction regions (Cashman et al., 2017; Gualda et al., 2019). On the other hand, our data do not exclude any role for dynamic reorganization during assembly of large magma bodies. In particular, hints of higher water concentrations recorded by plagioclase crystals from the Oruanui, Rotoiti, and early and middle Bishop Tuff eruptions may point to ascent and reequilibration of melt inclusions in an upper crustal storage region prior to eruption. This is consistent with evidence for decompression of Oruanui magmas to form a shallow magma chamber <1,600 yrs prior to eruption (Allan et al., 2013). Variations in melt viscosity as a function of chemical composition could further influence the degree of melt-crystal segregation and thus the reorganization of eruptible melt that takes place within crystal-rich magma reservoirs (e.g., Floess et al., 2019).

370

371

372

373

374

375

376

377

378

379

380

381

382

383

384

385

386

387

388

389

390

391

392

Depending on recharge, volatiles, and the rheology of the magma and surrounding rock (Townsend et al., 2019; Huber et al., 2019), magmatic systems can find their own trajectories—their own life cycles—that balance chamber growth, eruption, and freezing. How does the physical architecture of magmatic systems change through these life cycles? Our dataset comprises snapshots of magmatic systems of different sizes. Because the size of magma reservoirs is related to the thermomechanical regime of the magma and surrounding crust (e.g., Jellinek and DePaolo, 2003; Caricchi et al., 2014; Townsend et al., 2019; Huber et al., 2019), these snapshots can be mapped onto a regime diagram relating thermomechanical state to

eruption initiation mechanisms (Figure 7). This leads to the hypothesis that the thermomechanical state, eruption initiation mechanisms, and architecture of magmatic systems are all intertwined as depicted in Figure 7.

### 5. Conclusions

The structure of magma reservoirs is linked with mobility of bubbles and melt, rheological evolution of magma and surrounding rock, and triggering of eruptions (e.g., Cashman et al., 2017). Geophysical imaging techniques provide a means to characterize the vertical structure of upper crustal reservoirs in a range of settings, but large magma reservoirs may spend the majority of their lifetimes in subsolidus states (e.g., Rubin et al., 2017). Using petrologic records, we find that the magma reservoirs that feed caldera-forming eruptions are architecturally diverse, ranging from consolidated bodies to dispersed lenses that span the upper crust. Dispersed magma lenses tapped during eruptions are either spread out within a larger mush body or separated by country rock and solidified magma. The vertical structure of the magma bodies tapped during caldera-forming eruptions is scale-dependent, with a tendency towards vertically consolidated upper crustal reservoirs among the smallest (<10 km³ DRE) and largest (>500 km³ DRE) eruptions.

VS ratios calculated from rhyolite-MELTS geobarometry (Gualda and Ghiorso, 2014) agree with VS ratios based on melt inclusions. Magmatic water concentrations calculated from plagioclase-melt equilibria (Waters and Lange, 2015) also broadly agree with water concentrations in melt inclusions, further supporting the magmatic storage pressures inferred from melt inclusions. Coupled CaAl-NaSi interdiffusion in plagioclase is slow compared to re-

equilibration of water in melt inclusions (Grove et al., 1984; Qin et al., 1992), implying that melt inclusions reflect storage conditions just prior to eruption whereas plagioclase compositions offer a longer-term window into magma storage. We interpret agreement between melt inclusion and plagioclase records as evidence for a more static view of large magma bodies, in which consolidation takes place primarily through progressive emplacement of more magma into the upper crust rather than through upward migration of initially distributed magma bodies.

Potential eruption initiation mechanisms depend on the thermomechanical regime of the magmatic system, which in turn depends on magma chamber size (Jellinek and DePaolo, 2003; Degruyter and Huber, 2014; Townsend et al., 2019). Here we find evidence that the vertical architecture of upper crustal magmatic systems also varies systematically with the scale of the magmatic system. Consequently we hypothesize that changes in scale and thermomechanical regime develop and evolve in tandem with magmatic architecture through the life cycle of a magmatic system.

# **Acknowledgments and Data**

The compilation of melt inclusion water and CO<sub>2</sub> saturation pressures and the compilation of plagioclase compositions and glass/whole rock compositions are available as supplementary Excel spreadsheets accompanying this article. The authors thank Heather Wright for sharing an early version of the melt inclusion volatiles database, and Laura Waters for assistance with the plagioclase-melt hygrometer. We thank Michael Eddy and Luca Caricchi for constructive reviews that improved this manuscript, and Ben Ellis and an anonymous reviewer for feedback on an earlier version of this work. BAB thanks Kenny Befus, Chris Huber, Leif Karlstrom, Ben Klein, Marc-Antoine Longpré, Michael Manga, Tushar Mittal, Ayla Pamukcu, and the members of the City Volcano Lab for thought-provoking conversations. BAB is grateful for support from a PSC-CUNY award. We acknowledge support from NSF award 2015322.

442

449

450

451 452

453 454

455

456 457

458 459

460

461

462

463 464

465

466

467 468

469

470 471

472

473 474

475

476

477

References Cited

- Allan, A.S., Morgan, D.J., Wilson, C.J., and Millet, M., 2013, From mush to eruption in centuries: assembly of the super-sized Oruanui magma body: Contributions to Mineralogy and Petrology, v. 166, no. 1, p. 143-164.
- Andrews, B.J., and Gardner, J.E., 2010, Effects of caldera collapse on magma decompression rate: An example from the 1800 14 C yrBP eruption of Ksudach Volcano, Kamchatka, Russia: Journal of Volcanology and Geothermal Research, v. 198, no. 1, p. 205-216.
  - Annen, C., 2009, From plutons to magma chambers: Thermal constraints on the accumulation of eruptible silicic magma in the upper crust: Earth and Planetary Science Letters, v. 284, no. 3-4, p. 409-416.
  - Annen, C., Blundy, J., and Sparks, R., 2006, The genesis of intermediate and silicic magmas in deep crustal hot zones: Journal of Petrology, v. 47, no. 3, p. 505-539.
  - Bachmann, O., and Bergantz, G., 2008, The magma reservoirs that feed supereruptions: Elements, v. 4, no. 1, p. 17-21.
  - Bachmann, O., Wallace, P.J., and Bourquin, J., 2010, The melt inclusion record from the rhyolitic Kos Plateau Tuff (Aegean Arc): Contributions to Mineralogy and Petrology, v. 159, no. 2, p. 187.
    - Bacon, C.R., and Druitt, T.H., 1988, Compositional evolution of the zoned calcalkaline magma chamber of Mount Mazama, Crater Lake, Oregon: Contributions to Mineralogy and Petrology, v. 98, no. 2, p. 224-256.
    - Barker, S.J., Wilson, C.J., Allan, A.S., and Schipper, C.I., 2015, Fine-scale temporal recovery, reconstruction and evolution of a post-supereruption magmatic system: Contributions to Mineralogy and Petrology, v. 170, no. 1, p. 1-40.
    - Bégué, F., Gravley, D.M., Chambefort, I., Deering, C.D., and Kennedy, B.M., 2015, Magmatic volatile distribution as recorded by rhyolitic melt inclusions in the Taupo Volcanic Zone, New Zealand: Geological Society, London, Special Publications, v. 410, no. 1, p. 71-94.
    - Bégué, F., Gualda, G.A., Ghiorso, M.S., et al., 2014, Phase-equilibrium geobarometers for silicic rocks based on rhyolite-MELTS. Part 2: application to Taupo Volcanic Zone rhyolites: Contributions to Mineralogy and Petrology, v. 168, no. 5, p. 1082.
    - Black, B.A., and Manga, M., 2017, Volatiles and the tempo of flood basalt magmatism: Earth and Planetary Science Letters, v. 458, p. 130-140.
    - Cadoux, A., Scaillet, B., Druitt, T.H., and Deloule, E., 2014, Magma storage conditions of large Plinian eruptions of Santorini Volcano (Greece): Journal of Petrology, v. 55, no. 6, p. 1129-1171.
    - Caricchi, L., Annen, C., Blundy, J., Simpson, G., and Pinel, V., 2014, Frequency and magnitude of volcanic eruptions controlled by magma injection and buoyancy: Nature Geoscience, v. 7, no. 2, p. 126-130.
  - Caricchi, L., Sheldrake, T.E., and Blundy, J., 2018, Modulation of magmatic processes by CO 2 flushing: Earth and Planetary Science Letters, v. 491, p. 160-171.
- Cashman, K.V., and Giordano, G., 2014, Calderas and magma reservoirs: Journal of Volcanology and Geothermal Research, v. 288, p. 28-45.
- Cashman, K.V., Sparks, R.S., and Blundy, J.D., 2017, Vertically extensive and unstable magmatic systems: A unified view of igneous processes: Science (New York, N.Y.), v. 355, no. 6331, p. 10.1126/science.aag3055.
- Chamberlain, K., Wilson, C., Wallace, P., and Millet, M., 2015, Micro-analytical perspectives on the Bishop Tuff and its magma chamber: Journal of Petrology, v. 56, no. 3, p. 605-640.
- Chesner, C.A., and Luhr, J.F., 2010, A melt inclusion study of the Toba Tuffs, Sumatra, Indonesia: Journal of Volcanology and Geothermal Research, v. 197, no. 1, p. 259-278.
- Cooper, G.F., Wilson, C.J., Millet, M., Baker, J.A., and Smith, E.G., 2012, Systematic tapping of independent magma chambers during the 1Ma Kidnappers supercruption: Earth and Planetary Science Letters, v. 313, p. 23-33.

Degruyter, W., and Huber, C., 2014, A model for eruption frequency of upper crustal silicic magma chambers: Earth and Planetary Science Letters, v. 403, p. 117-130.

499

500 501

502

503

504

505

506 507

511512

- Di Muro, A., Villemant, B., Montagnac, G., Scaillet, B., and Reynard, B., 2006, Quantification of water content and speciation in natural silicic glasses (phonolite, dacite, rhyolite) by confocal microRaman spectrometry: Geochimica et Cosmochimica Acta, v. 70, no. 11, p. 2868-2884.
- Druitt, T., Costa, F., Deloule, E., Dungan, M., and Scaillet, B., 2012, Decadal to monthly timescales of magma transfer and reservoir growth at a caldera volcano.
- Eddy, M.P., Bowring, S.A., Miller, R.B., and Tepper, J.H., 2016, Rapid assembly and crystallization of a fossil large-volume silicic magma chamber: Geology, v. 44, no. 4, p. 331-334.
  - Floess, D., Caricchi, L., Simpson, G., and Wallis, S.R., 2019, Melt segregation and the architecture of magmatic reservoirs: insights from the Muroto sill (Japan): Contributions to Mineralogy and Petrology, v. 174, no. 4, p. 27.
  - Geyer, A., and Marti, J., 2008, The new worldwide collapse caldera database (CCDB): A tool for studying and understanding caldera processes: Journal of Volcanology and Geothermal Research, v. 175, no. 3, p. 334-354.
  - Gregg, P.M., Silva, S.d., Grosfils, E.B., and Parmigiani, J.P., 2012, Catastrophic caldera-forming eruptions: Thermomechanics and implications for eruption triggering and maximum caldera dimensions on Earth: Journal of Volcanology and Geothermal Research, v. 241-242, p. 1-12.
- Grove, T.L., Baker, M.B., and Kinzler, R.J., 1984, Coupled CaAl-NaSi diffusion in plagioclase feldspar: experiments and applications to cooling rate speedometry: Geochimica et Cosmochimica Acta, v. 48, no. 10, p. 2113-2121.
  - Gualda, G.A., and Ghiorso, M.S., 2014, Phase-equilibrium geobarometers for silicic rocks based on rhyolite-MELTS. Part 1: Principles, procedures, and evaluation of the method: Contributions to Mineralogy and Petrology, v. 168, no. 1, p. 1033.
- Gualda, G.A., Gravley, D.M., Connor, M., et al., 2018, Climbing the crustal ladder: Magma storage-depth evolution during a volcanic flare-up: Science advances, v. 4, no. 10, p. eaap7567.
- Gualda, G.A.R., Gravley, D.M., Deering, C.D., and Ghiorso, M.S., 2019, Magma extraction pressures and the architecture of volcanic plumbing systems 522, 118 p.
- Gudmundsson, M.T., Jonsdottir, K., Hooper, A., et al., 2016, Gradual caldera collapse at Bardarbunga volcano, Iceland, regulated by lateral magma outflow: Science (New York, N.Y.), v. 353, no. 6296, p. aaf8988.
- Hattori, K., and Sato, H., 1996: Magma evolution recorded in plagioclase zoning in 1991 Pinatubo eruption products.
- Hildreth, W., 1981, Gradients in silicic magma chambers: implications for lithospheric magmatism: Journal of Geophysical Research: Solid Earth, v. 86, no. B11, p. 10153-10192.
- Hildreth, W., and Fierstein, J., 2000, Katmai volcanic cluster and the great eruption of 1912: Geological Society of America Bulletin, v. 112, no. 10, p. 1594-1620.
- Huber, C., Townsend, M., Degruyter, W., and Bachmann, O., 2019, Optimal depth of subvolcanic magma chamber growth controlled by volatiles and crust rheology: Nature Geoscience, v. 12, no. 9, p. 762-768.
- Iacovino, K., Ju-Song, K., Sisson, T., et al., 2016, Quantifying gas emissions from the "Millennium Eruption" of Paektu volcano, Democratic People's Republic of Korea/China: Science Advances, v. 2, no. 11, p. e1600913.
- Jaxybulatov, K., Shapiro, N.M., Koulakov, I., Mordret, A., Landes, M., and Sens-Schonfelder, C., 2014, Volcanology. A large magmatic sill complex beneath the Toba caldera: Science (New York, N.Y.), v. 346, no. 6209, p. 617-619.
- Jellinek, A.M., and DePaolo, D.J., 2003, A model for the origin of large silicic magma chambers: precursors of caldera-forming eruptions: Bulletin of Volcanology, v. 65, no. 5, p. 363-381.
- Johnson, E.R., Kamenetsky, V.S., McPhie, J., and Wallace, P.J., 2011, Degassing of the H2O-rich rhyolites of the Okataina Volcanic Center, Taupo Volcanic Zone, New Zealand: Geology, v. 39, no. 4, p. 311-314.

- Karlstrom, L., Rudolph, M.L., and Manga, M., 2012, Caldera size modulated by the yield stress within a crystal-rich magma reservoir: Nature Geoscience, v. 5, no. 6, p. 402-405.
- Lipman, P.W., 1997, Subsidence of ash-flow calderas: relation to caldera size and magma-chamber geometry: Bulletin of volcanology, v. 59, no. 3, p. 198-218.

548

549

550

551552

555

556

559560

561

562563

566

567

570571

572

576

577

578579

580

583

584

- Lowenstern, J.B., 1993, Evidence for a copper-bearing fluid in magma erupted at the Valley of Ten Thousand Smokes, Alaska: Contributions to Mineralogy and Petrology, v. 114, no. 3, p. 409-421.
  - Lu, Z., Wicks, C., Dzurisin, D., Thatcher, W., Freymueller, J.T., McNutt, S.R., and Mann, D., 2000, Aseismic inflation of Westdahl volcano, Alaska, revealed by satellite radar interferometry: Geophysical Research Letters, v. 27, no. 11, p. 1567-1570.
  - Mandeville, C.W., Webster, J.D., Tappen, C., et al., 2009, Stable isotope and petrologic evidence for open-system degassing during the climactic and pre-climactic eruptions of Mt. Mazama, Crater Lake, Oregon: Geochimica et Cosmochimica Acta, v. 73, no. 10, p. 2978-3012.
- Marianelli, P., Sbrana, A., and Proto, M., 2006, Magma chamber of the Campi Flegrei supervolcano at the time of eruption of the Campanian Ignimbrite: Geology, v. 34, no. 11, p. 937-940.
  - Marsh, B.D., 1982, On the mechanics of igneous diapirism, stoping, and zone melting: American Journal of Science, v. 282, no. 6, p. 808-855.
- Michaut, C., and Jaupart, C., 2006, Ultra-rapid formation of large volumes of evolved magma: Earth and Planetary Science Letters, v. 250, no. 1, p. 38-52.
  - Myers, M.L., Wallace, P.J., Wilson, C.J., Morter, B.K., and Swallow, E.J., 2016, Prolonged ascent and episodic venting of discrete magma batches at the onset of the Huckleberry Ridge supereruption, Yellowstone: Earth and Planetary Science Letters, v. 451, p. 285-297.
  - Newman, S., and Lowenstern, J.B., 2002, VolatileCalc: a silicate melt–H 2 O–CO 2 solution model written in Visual Basic for Excel: Computers & Geosciences, v. 28, no. 5, p. 597-604.
- Pamukcu, A.S., Ghiorso, M.S., and Gualda, G.A., 2016, High-Ti, bright-CL rims in volcanic quartz: a result of very rapid growth: Contributions to Mineralogy and Petrology, v. 171, no. 12, p. 105.
  - Qin, Z., Lu, F., and Anderson, A.T., 1992, Diffuse reequilibration of melt and fluid inclusions: The American mineralogist, v. 77, no. 5-6, p. 565-576.
- Rubin, A.E., Cooper, K.M., Till, C.B., et al., 2017, Rapid cooling and cold storage in a silicic magma reservoir recorded in individual crystals: Science, v. 356, no. 6343, p. 1154-1156.
  - Schmitz, M.D., and Smith, I.E., 2004, The petrology of the Rotoiti eruption sequence, Taupo Volcanic Zone: an example of fractionation and mixing in a rhyolitic system: Journal of Petrology, v. 45, no. 10, p. 2045-2066.
- 573 Smith, V., Shane, P., and Nairn, I., 2010, Insights into silicic melt generation using plagioclase, quartz 574 and melt inclusions from the caldera-forming Rotoiti eruption, Taupo volcanic zone, New Zealand: 575 Contributions to Mineralogy and Petrology, v. 160, no. 6, p. 951-971.
  - Tait, S., Jaupart, C., and Vergniolle, S., 1989, Pressure, gas content and eruption periodicity of a shallow, crystallising magma chamber: Earth and Planetary Science Letters, v. 92, no. 1, p. 107-123.
  - Townsend, M., Huber, C., Degruyter, W., and Bachmann, O., 2019, Magma chamber growth during inter-caldera periods: insights from thermo-mechanical modeling with applications to Laguna del Maule, Campi Flegrei, Santorini, and Aso: Geochemistry, Geophysics, Geosystems.
- Venezky, D.Y., and Rutherford, M.J., 1999, Petrology and Fe–Ti oxide reequilibration of the 1991 Mount Unzen mixed magma: Journal of Volcanology and Geothermal Research, v. 89, no. 1-4, p. 213-230.
  - Wallace, P.J., Anderson, A.T., and Davis, A.M., 1999, Gradients in H2O, CO2, and exsolved gas in a large-volume silicic magma system: Interpreting the record preserved in melt inclusions from the Bishop Tuff: Journal of Geophysical Research: Solid Earth, v. 104, no. B9, p. 20097-20122.
- Wallace, P.J., and Gerlach, T.M., 1994, Magmatic vapor source for sulfur dioxide released during
   volcanic eruptions: evidence from mount pinatubo: Science (New York, N.Y.), v. 265, no. 5171, p.
   497-499.
- Waters, L.E., and Lange, R.A., 2015, An updated calibration of the plagioclase-liquid hygrometerthermometer applicable to basalts through rhyolites: American Mineralogist, v. 100, no. 10, p. 2172-2184.

Wilson, C., Blake, S., Charlier, B., and Sutton, A., 2005, The 26·5 ka Oruanui eruption, Taupo volcano,
New Zealand: development, characteristics and evacuation of a large rhyolitic magma body: Journal
of Petrology, v. 47, no. 1, p. 35-69.

# Figures and captions

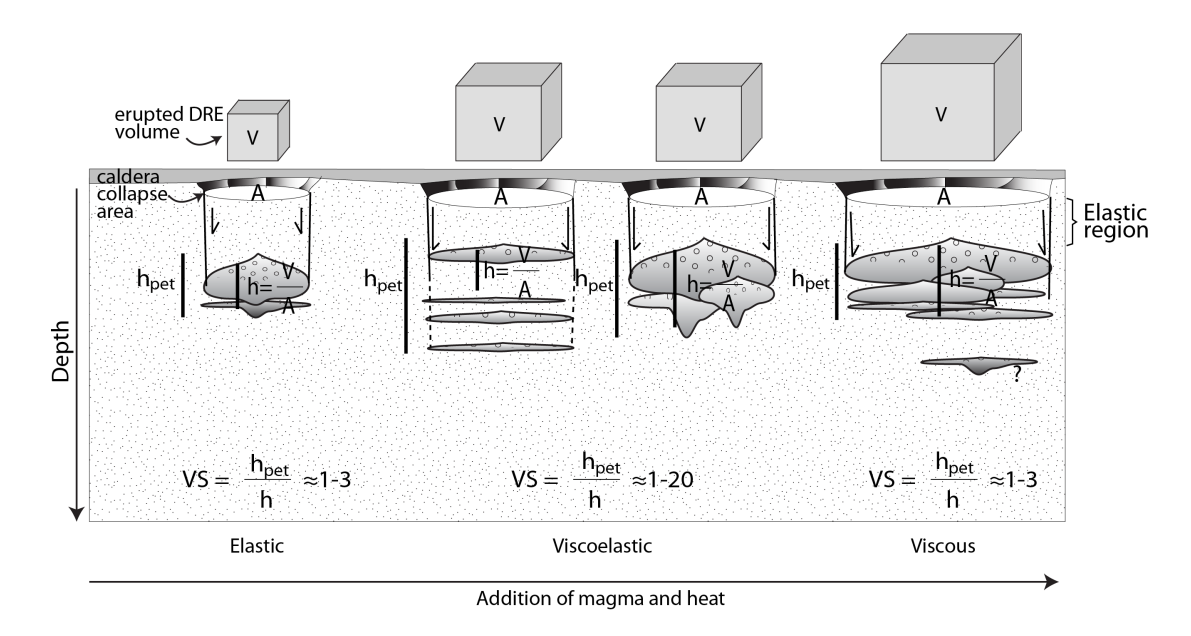


**Figure 1.** Cartoon illustrating the Vertical Separation (VS) ratio, and how it reflects the vertical structures of the upper crustal portions of the magmatic systems that feed caldera-forming eruptions. For simplicity, dikes and lower and middle crustal portions of the magmatic system are not shown here.

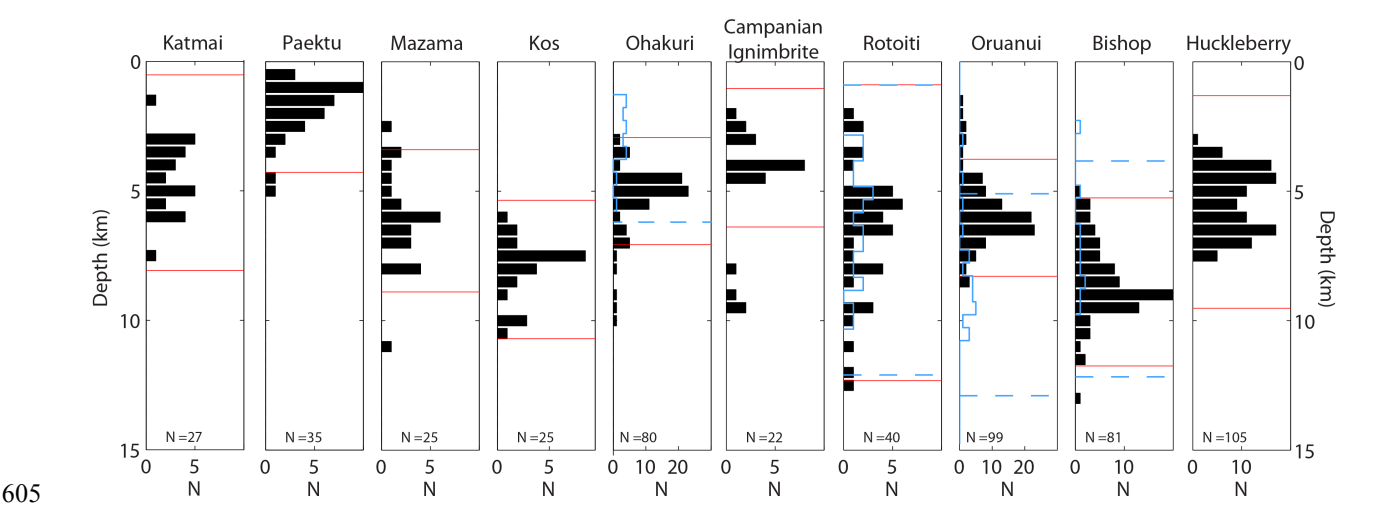
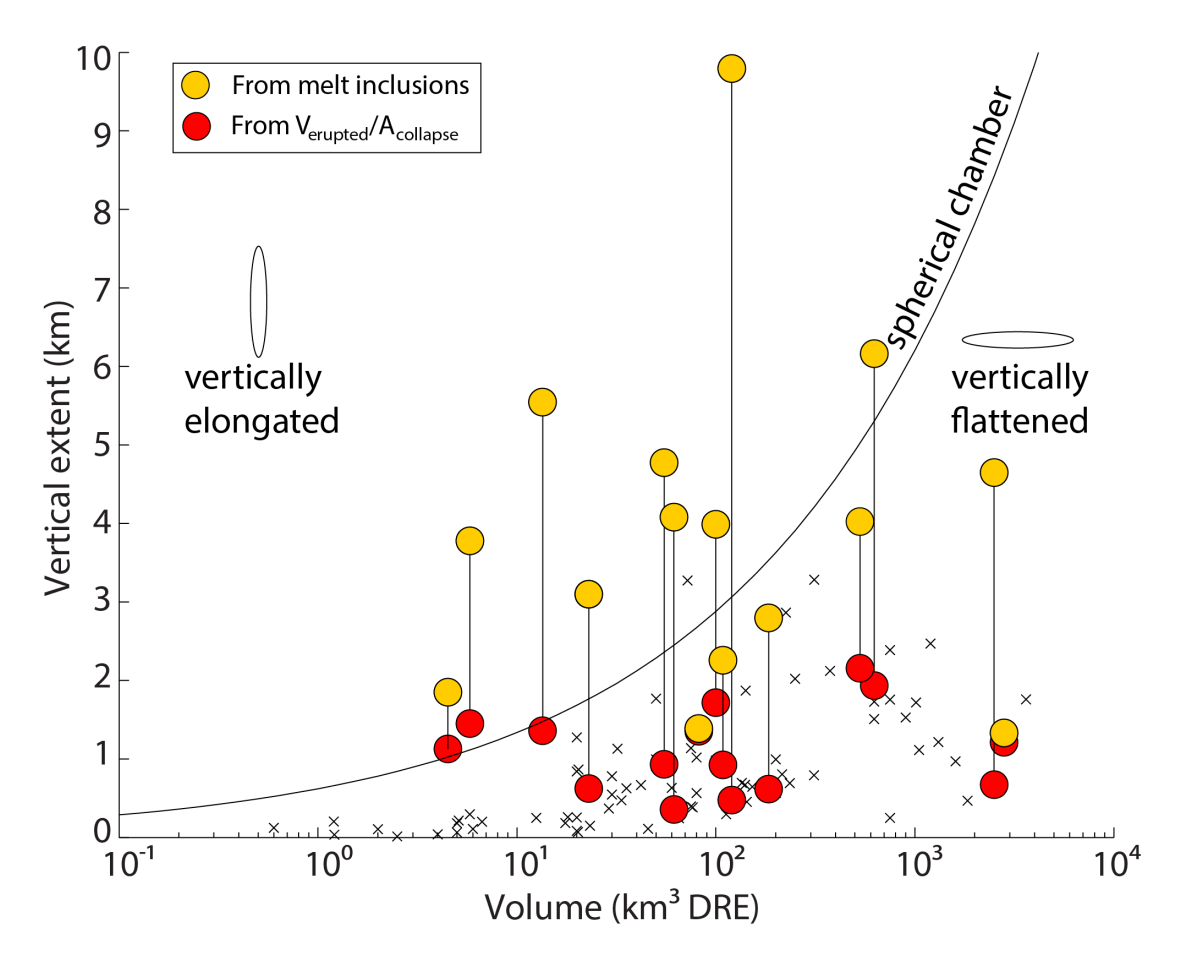


Figure 2. Melt inclusions record distributions of entrapment pressures that reflect the vertical structure of the reservoir system in which magma resided (and within which melt inclusions were entrapped and equilibrated) prior to eruption. Here we show distributions of saturation depths for magmatic systems for which at least 20 melt inclusion data points are available (references in text and Table 1; plots for eruptions with fewer than 20 melt inclusions are shown in Supplementary Figure 1). Red lines indicate cutoffs for depth calculated as 1.5 times the interquartile range above and below the third and first quartile, respectively (see text for details). Blue solid and dashed lines indicate distributions and interquartile cutoffs respectively for rhyolite-MELTS pressure estimates (Supplementary Table 1).



**Figure 3.** Vertical extent of pre-eruptive reservoirs inferred from erupted volumes and caldera footprints. Consolidated vertical extents, shown with black crosses from Geyer and Marti (2008) and red circles from our compilation, are compared with vertical extent reflected in the range of melt inclusion saturation pressures (yellow circles). After Cashman and Giordano (2014).

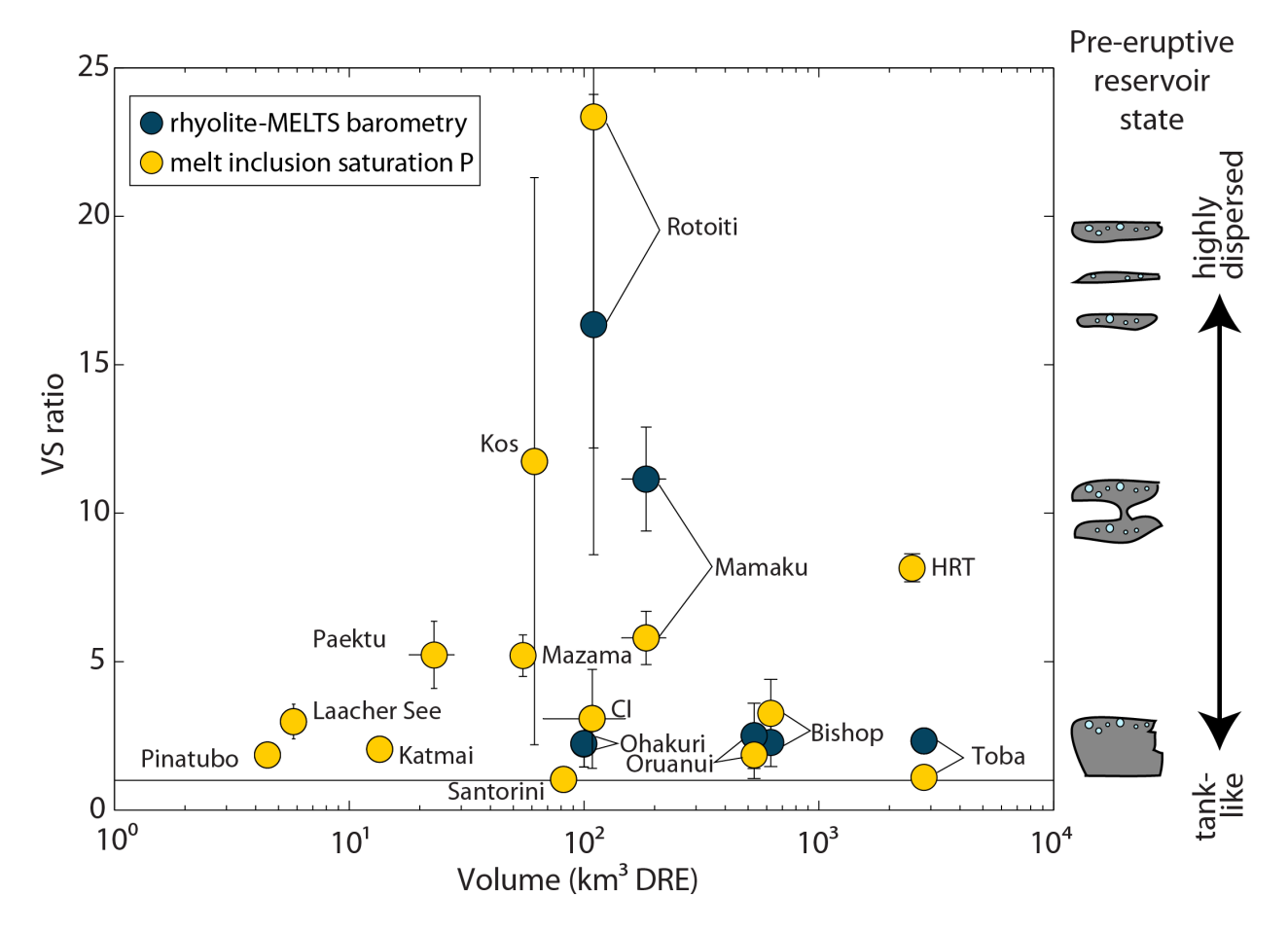


Figure 4. Vertical structures of the magma reservoirs that feed caldera-forming eruptions are diverse, ranging from vertically compact equant shapes to vertically dispersed lenses to high aspect ratio, vertically compact, consolidated magma bodies. The ratios of vertical extent from melt inclusion saturation pressures (light yellow) and rhyolite-MELTS barometry (dark navy, from Gualda and Ghiorso (2014); Bégué et al. (2014), and Gualda et al. (2018)) relative to the consolidated vertical extent shows that intermediate-scale eruptions in particular tap vertically distributed reservoir systems. Rhyolite-MELTS barometry for the Ohakuri, Mamaku, and Toba eruptions is based on matrix glass compositions; rhyolite-MELTS barometry for the Oruanui, Rotoiti, and Bishop Tuff eruptions is based on melt inclusion glass compositions (Supplementary Table 1). The large uncertainty in VS ratio for the Kos Plateau Tuff reflects uncertainty in caldera collapse area.

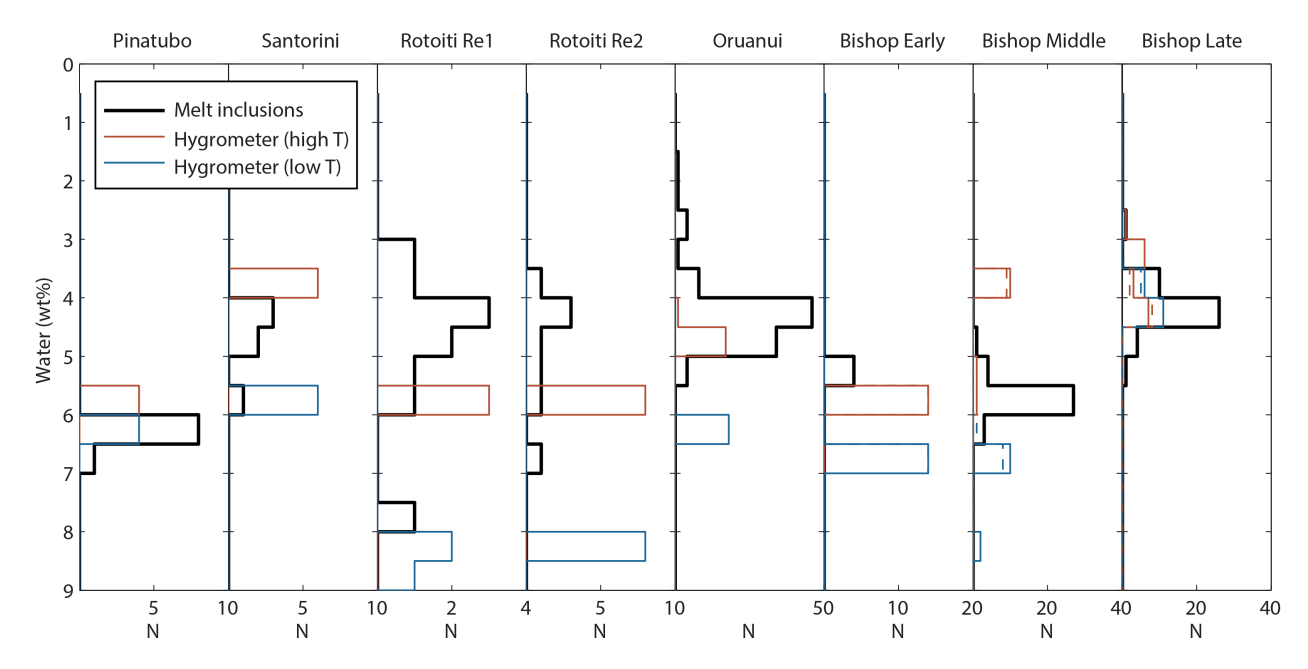
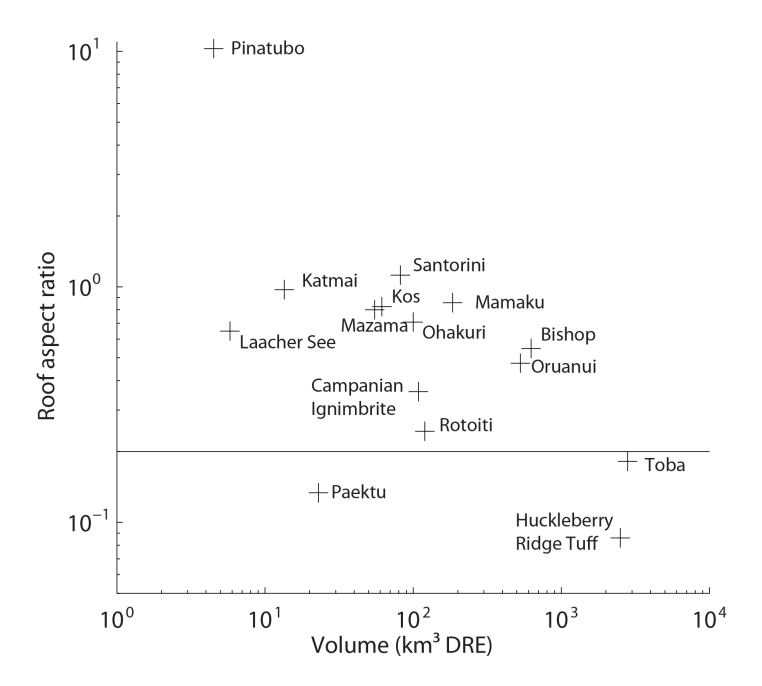


Figure 5. Comparison of water concentrations measured in melt inclusions relative to water concentrations calculated with the plagioclase-liquid hygrometer of Waters and Lange (2015). Data sources in text, Table 2, and Supplementary Table 2. Solid lines indicate water concentrations calculated from plagioclase rim compositions and matrix glasses; dashed lines (Bishop Tuff only) indicate water concentrations calculated from plagioclase core compositions and matrix glasses. The plagioclase-liquid hygrometer gives H<sub>2</sub>O concentration in the melt, whereas melt inclusions give H<sub>2</sub>O and CO<sub>2</sub> concentrations in the melt, and depth estimates are calculated from combined H<sub>2</sub>O and CO<sub>2</sub> concentrations (CO<sub>2</sub> is reported). Therefore we compare water concentrations rather than depths in this figure, because depths estimated from water concentrations given by the hygrometer would represent minimum depths compared with those estimated from melt inclusions.



**Figure 6.** Roof aspect ratios for caldera-forming eruptions. The roof aspect ratio =  $D_{top}/a$ , where  $D_{top}$  is the depth to the top of the magma chamber, excluding any outliers as defined in the text, and a is the horizontal half-width of the magma chamber, calculated as  $a = \sqrt{A_{collapse}/\pi}$ . The critical roof aspect ratio (Gregg et al., 2012) for roof failure (~0.2) is shown as a horizontal solid line.

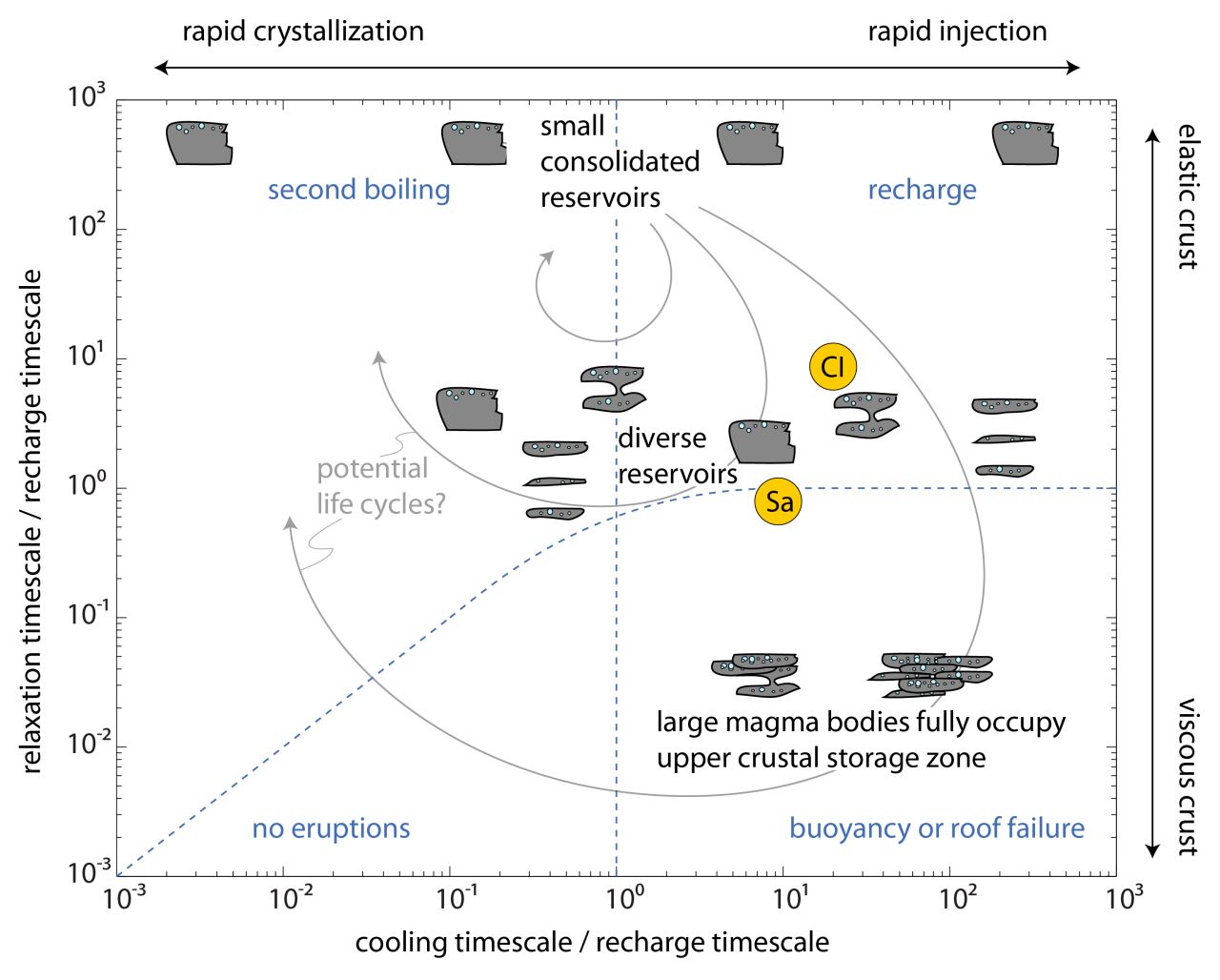


Figure 7. Hypothesized regime diagram linking thermomechanical evolution of magma chambers with reservoir structure. Regime diagram modified from Degruyter and Huber (2014) and Townsend et al. (2019), with eruption trigger mechanisms indicated in blue text and approximate regime boundaries demarcated by dashed lines. Sa=Santorini pre-Minoan thermomechanical regime and CI=Campi Flegrei Epoch 2 thermomechanical regime, as determined by Townsend et al. (2019). The hypothesized evolution of reservoir architecture is based on thermomechanical considerations—namely that as magma chambers grow the overall magmatic system is expected to shift from an elastic to viscous regime—combined with the data in Figure 4, which constrain the architecture of magmatic systems of different sizes. The potential trajectories through the life cycle of a magmatic system are intended as idealized

- 669 hypotheses. Some systems are likely to follow trajectories in which they do not experience a
- large eruption until late in their life cycles; others may never progress beyond small,
- consolidated magma reservoirs.